Fast Rydberg antiblockade regime and its applications in quantum logic gates

Shi-Lei Su (苏石磊),[1,*] Ya Gao (郜雅),[1] Erjun Liang (梁二军),[1,†] and Shou Zhang (张寿)[2]

[1]*School of Physical Science and Engineering and Key Laboratory of Materials Physics of Ministry of Education of China, Zhengzhou University, Zhengzhou 450052, People's Republic of China*

[2]*Department of Physics, College of Science, Yanbian University, Yanji, Jilin 133002, People's Republic of China*

(Received 12 November 2016; published 13 February 2017)

Unlike the Rydberg blockade regime, the Rydberg antiblockade regime (RABR) allows more than one Rydberg atom to be excited, which can bring other interesting phenomena and applications. We propose an alternative scheme to quickly achieve the RABR. The proposed RABR can be implemented by adjusting the detuning of the classical driving field, which is, in turn, based on the former numbers of the excited Rydberg atoms. In contrast to the former schemes, the current one enables more than two atoms to be excited to Rydberg states in a short period of time and thus is useful for large-scale quantum information processing. The proposed RABR can be used to construct two- and multiqubit quantum logic gates. In addition, a Rydberg excitation superatom, which can decrease the blockade error and enlarge the blockade radius for Rydberg blockade-based schemes, is constructed based on the suggested RABR and used to realize a more robust quantum logic gate. The mechanical effect and the ionization are discussed, and the performance is investigated using the master-equation method. Finally, other possible applications of the present RABR are also given.

DOI: 10.1103/PhysRevA.95.022319

I. INTRODUCTION

Rydberg atoms have state-dependent interaction properties and are thus useful for quantum information processing [1,2]. If atoms are in a Rydberg state and close enough, they will interact directly and strongly with each other due to their large electric dipole, and the collective jumped Rydberg states would be shifted by some amount of energy depending on the distance between them. Consequently, a classical laser field driving a ground state to the Rydberg state cannot excite both atoms at the same time [3,4] when the linewidth of the excitation is significantly narrower than the energy shift, which is well known as Rydberg blockage. This effect turns the Rydberg atoms into a collectively two-level system; that is, all of the Rydberg atoms are in their ground state, or one and only one of them is excited. Experimentally, Tong *et al.* [5], Singer *et al.* [6], and Cubel Liebisch *et al.* [7] previously observed a suppression of the excitation in the Rydberg gas as a function of laser intensity and atom density. Subsequently, evidence of coherent collective Rydberg excitation of frozen Rydberg gases in the strong blockade regime has also been found [8]. Also, a blockade with two Rydberg atoms located about 10 μm [9] and 4 μm [10] apart has been observed. Recently, researchers have successfully observed entanglement between neutral atoms [11], cooperative optical nonlinearity [12], collective many-body quantum dynamics [13–15], and energy transport under the influence of a controlled environment [16] induced by a Rydberg blockade. The Rydberg blockade effect offers many possibilities for realizing two- [17–27] and multiqubit [28–30] quantum logic gates. Although multiqubit quantum logic gates can be decomposed into a sequence of single-qubit operations and two-qubit universal logic gates [31], implementing them directly still has significance for quantum computation since many quantum resources would be saved.

In contrast to the blockade regime, a so-called Rydberg antiblockade regime (RABR) was recently proposed by Ates *et al.* [32] in an ultracold lattice gas. An increased two-photon Rydberg excitation probability in a three-level scheme was predicted when interaction energy matches the Rabi frequency of the lower transition. In the scheme, the lattice was considered with a fixed lattice constant, while the interaction strength between the Rydberg atoms was tuned by changing the principal quantum number. Subsequently, the RABR was demonstrated experimentally [33]. Starting from an unstructured gas, Amthor *et al.* [33] showed that, even at interatomic separations where the atomic interaction shift is much greater than the excitation linewidth, atomic pairs can also be resonantly excited. In contrast to Ref. [32], Ref. [33] kept the quantum number fixed, while the strength of the Rydberg interaction was instead matched by selecting specific atom pairs with the proper interatomic distance. Although the population of the two-atom Rydberg excited state P_{rr} is not higher than 12% [32] or 20% [33], these schemes pave the way for an antiblockade regime of Rydberg atoms. In addition, Pohl and Berman found that, when the number of Rydberg atoms (each atom has three Rydberg energy levels) was increased from two to three, the system would undergo the antiblockade regime once the dark state containing three excited Rydberg atoms with different Rydberg states was populated [34]. Based on the model studied in Ref. [34], Qian *et al.* showed that the breakdown of the dipole blockade can occur between two Rydberg atoms when they are interacting with a zero-area phase-jump pulse [35].

Unlike the former antiblockade schemes, Zuo and Nakagawa [36] and Lee *et al.* [37] gave critical conditions to achieve the resonant transition between collective Rydberg excited states and ground states. By adjusting the detuning between the driving field and atomic transition frequencies to make it fulfill some specific conditions, the energy shift induced by Rydberg interaction can be compensated, and thus,

*slsu@zzu.edu.cn
†ejliang@zzu.edu.cn

the resonant transition is achieved. Subsequently, by combing the advantages of dissipative dynamics, Carr and Saffman [38] proposed a scheme to obtain the steady entanglement of two Rydberg atoms under the antiblockade regime. In addition, the RABR-based schemes to realize two-qubit universal quantum logic gate were also presented [39,40].

However, the RABR mentioned above is valid only for two Rydberg atoms [37–40]. Although Ref. [36] can achieve the multiatom excitation between nearest-neighbor interacting atoms on the time scale Δ/Ω^2 (Δ and Ω denote the detuning and Rabi frequency of the laser, respectively, and $\Delta \gg \Omega$), it would be more interesting if one could achieve the multiqubit RABR on a shorter time scale $1/\Omega$ when considering the interactions between any two Rydberg atoms. Inspired by this, we design an alternative scheme to realize the multiqubit RABR in a short period of time and mainly show its applications in quantum logic gates.

II. REVIEW OF RYDBERG BLOCKADE AND ANTIBLOCKADE WITH SIMULTANEOUS DRIVING

A. Rydberg blockade regime

Let us review how the presence of Rydberg interactions induces the blockade regime.

As shown in Fig. 1(a), we consider two identical Rydberg atoms. Each of the atoms has one Rydberg state $|r\rangle$ and one ground state $|1\rangle$. The transition $|1\rangle \leftrightarrow |r\rangle$ is driven by the classical field resonantly with Rabi frequency Ω. The Rydberg-Rydberg-interaction (RRI) strength is V. Therefore, in the interaction picture, the Hamiltonian of the system can be written as (setting $\hbar = 1$)

$$\hat{H} = \frac{\Omega}{2}(|1\rangle_1\langle r| \otimes \hat{\mathcal{I}}_2 + \hat{\mathcal{I}}_1 \otimes |1\rangle_2\langle r| + \text{H.c.}) + V|rr\rangle\langle rr|, \tag{1}$$

where the subscripts 1 and 2 denote the transitions of atoms 1 and 2, respectively. $\hat{\mathcal{I}}_i$ is the identity operator of atom i. $|mn\rangle$ is the abbreviation of $|m\rangle_1|n\rangle_2$, and we will use this type of abbreviation throughout this paper. Under the basis $\{|11\rangle, |T\rangle, |rr\rangle\}$, the Hamiltonian can be rewritten as

$$\hat{H} = \frac{\sqrt{2}\Omega}{2}(|11\rangle\langle T| + |T\rangle\langle rr| + \text{H.c.}) + V|rr\rangle\langle rr|. \tag{2}$$

After moving Eq. (2) to the rotating frame with respect to $\hat{U} \equiv e^{-iV|rr\rangle\langle rr|t}$, one can get

$$\begin{aligned}\hat{H}' &= i\frac{d\hat{U}^+}{dt}\hat{U} + \hat{U}^+\hat{H}\hat{U} \\ &= \frac{\sqrt{2}\Omega}{2}(|11\rangle\langle T| + |T\rangle\langle rr|e^{-iVt} + \text{H.c.}).\end{aligned} \tag{3}$$

If parameters satisfy $V \gg \sqrt{2}\Omega/2$, the terms oscillating fast can be ignored safely. That is, the doubly excited Rydberg state $|rr\rangle$ cannot be pumped from $|T\rangle$, which is well known as the Rydberg blockade. Nevertheless, $|T\rangle$, which has one Rydberg state, can be pumped from $|11\rangle$ [Fig. 1(b)].

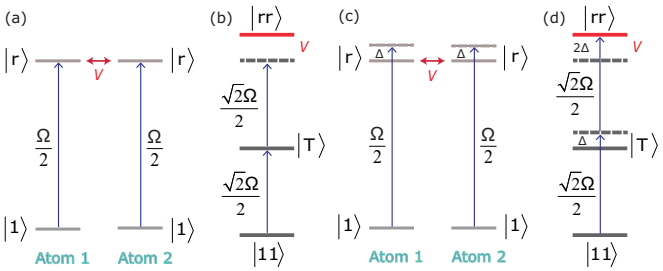

FIG. 1. Illustration of Rydberg blockade [(a), (b)] and antiblockade [(c), (d)] regimes with simultaneous driving. Each of the two atoms has one ground state $|1\rangle$ and one Rydberg state $|r\rangle$. The strength of the Rydberg interaction is V. The coupling strength between the Rydberg atom and the classical field is Ω. (a) [(c)] shows two interacting Rydberg atoms with resonant (large-detuned) driving. The transition $|1\rangle \leftrightarrow |r\rangle$ couples the laser resonantly [(a)] or dispersively [(c)] with blue detuning Δ. (b) [(d)] shows the effective coupling processes of (a) [(c)] in the two-atom basis $\{|11\rangle, |T\rangle, |rr\rangle\}$, in which $|T\rangle = (|1r\rangle + |r1\rangle)/\sqrt{2}$.

B. Rydberg antiblockade regime with simultaneous driving

In this section, we describe the RABR with simultaneous driving. As pointed out in Refs. [36–38], in the two-atom basis, if one were to adjust the laser frequency to be resonant to the shifted energy level $|rr\rangle$ [Fig. 1(d)], the RABR would emerge. To do this, the laser should drive the atom dispersively [Fig. 1(c)]. A more detailed explanation of RABR is as follows. In the interaction picture, the Hamiltonian can be written as

$$\begin{aligned}\hat{H} = &\frac{\Omega}{2}[(|1\rangle_1\langle r| \otimes \hat{\mathcal{I}}_2 + \hat{\mathcal{I}}_1 \otimes |1\rangle_2\langle r|)e^{i\Delta t} + \text{H.c.}] \\ &+ V|rr\rangle\langle rr|.\end{aligned} \tag{4}$$

After moving Eq. (4) to the rotating frame with respect to $\hat{U} \equiv e^{-iV|rr\rangle\langle rr|t}$, one can get

$$\hat{H}' = \frac{\sqrt{2}\Omega}{2}[|11\rangle\langle T|e^{i\Delta t} + |T\rangle\langle rr|e^{i(\Delta - V)t} + \text{H.c.}] \tag{5}$$

in the two-atom basis $\{|11\rangle, |T\rangle, |rr\rangle\}$, in which $|T\rangle = (|1r\rangle + |r1\rangle)/\sqrt{2}$. Then, if parameters satisfy $\Delta = V/2$ [36–38] and $\Delta \gg \sqrt{2}\Omega/2$, one can get the effective Hamiltonian [41],

$$\hat{H}'_{\text{eff}} = \frac{\Omega^2}{2\Delta}[(|11\rangle + |rr\rangle)(\langle 11| + \langle rr|) - 2|T\rangle\langle T|], \tag{6}$$

which can be further simplified to

$$\hat{H}'_{\text{eff}} = \frac{\Omega^2}{2\Delta}[(|11\rangle + |rr\rangle)(\langle 11| + \langle rr|)] \tag{7}$$

if the initial state is $|11\rangle$. It is easy to verify that $|11\rangle$ would be converted to $-|rr\rangle$ at the time $t = \pi\Delta/\Omega^2$ under the control of Eq. (7). In other words, the Rydberg blockade regime is broken, and the RABR emerges.

In what follows, we propose an alternative scheme to achieve RABR that allows two and multiple atoms to be excited in a short period of time. Also, we show that the present RABR can be used to construct two- and multiqubit quantum controlled-PHASE gates. Furthermore, based on the present RABR, we construct the "Rydberg excitation superatom", which can decrease the blockade error and enlarge the blockade radius for Rydberg blockade-based schemes.

III. RYDBERG ANTIBLOCKADE REGIME WITH SEQUENT DRIVING

A. Two-qubit case

As shown in Fig. 2(a), we consider two Rydberg atoms interacting with each other with strength V. The transition $|1\rangle_1 \leftrightarrow |r\rangle_1$ is driven resonantly by a π pulse with Rabi frequency Ω. Subsequently, the transition $|1\rangle_2 \leftrightarrow |r\rangle_2$ is driven dispersively by a π pulse with blue detuning Δ with the same Rabi frequency. In the interaction picture, the Hamiltonians of atoms 1 and 2 can be written as

$$\hat{H}_1 = \frac{\Omega}{2}(|1\rangle_1\langle r| + \text{H.c.}) \tag{8}$$

and

$$\hat{H}_2 = \frac{\Omega}{2}(|1\rangle_2\langle r|e^{i\Delta t} + \text{H.c.}), \tag{9}$$

respectively. The Rydberg interaction is described as

$$\hat{\mathcal{U}} = V|rr\rangle\langle rr|. \tag{10}$$

Suppose the initial state is $|11\rangle$; the whole process to realize two-atom RABR can be illustrated as follows.

(1) Apply a resonant π pulse on atom 1. Under the control of Hamiltonian (8), one can get the transition $|11\rangle \rightarrow -i|r1\rangle$.

(2) Apply a dispersive π pulse on atom 2 with blue detuning Δ. Then, the total Hamiltonian is changed to $\hat{H} = \hat{\mathcal{I}}_1 \otimes \hat{H}_2 + \hat{\mathcal{U}}$, which can be rewritten as

$$\hat{H} = \frac{\Omega}{2}(|r1\rangle\langle rr|e^{i(\Delta - V)t} + \text{H.c.}) \tag{11}$$

under the basis $\{|r1\rangle, |rr\rangle\}$ and after rotating with respect to $\hat{U} \equiv e^{-iV|rr\rangle\langle rr|t}$. If the antiblockade condition $\Delta = V$ is fulfilled, the transition $|r1\rangle \rightarrow -i|rr\rangle$ is generated, and thus, the RABR is achieved. The required time for the present RABR is $t = 2\pi/\Omega$, which is far shorter than that for the RABR with simultaneous driving.

B. Multiqubit case

In this section, we give the descriptions of the multiqubit RABR as shown in Fig. 2(b). Suppose any two of the Rydberg atoms interact with each other with the same RRI strength V. In the interest of simplicity, we first consider the three-qubit case. Suppose the initial state of the whole system is $|111\rangle$. Under the basis $\{|111\rangle, |r11\rangle, |rr1\rangle, |rrr\rangle\}$, the process to achieve three-qubit RABR can be illustrated as follows.

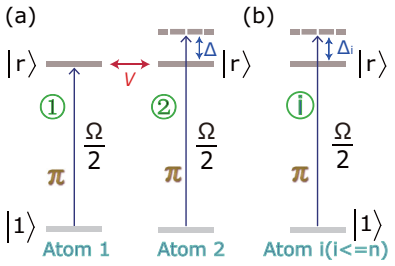

FIG. 2. Illustration of the RABR. Each of the atoms has one Rydberg state $|r\rangle$ and one ground state $|1\rangle$. (a) Two-qubit case. The transition $|1\rangle_{1(2)} \leftrightarrow |r\rangle_{1(2)}$ is driven by a classical laser resonantly (dispersively with blue detuning Δ), in which the numbers ($k = 1, 2$) mean the transition of atom k. (b) Multiqubit case. We suppose RRI strengths (denoted by V) between any two atoms equal each other. The antiblockade condition is, for the ith atom, $\Delta_i = (i-1)V$. The circles with numbers denote the steps.

(1) Apply a resonant π pulse on atom 1. One can get the transition $|111\rangle \rightarrow -i|r11\rangle$.

(2) Apply a dispersive π pulse on atom 2 with blue detuning $\Delta_2 = V$. Then the Hamiltonian of atom 2 in the interaction picture is $\hat{H}_2 = \frac{\Omega}{2}(|1\rangle_2\langle r|e^{i\Delta_2 t} + \text{H.c.})$, and that of the whole system is

$$\hat{H} = \frac{\Omega}{2}(|r11\rangle\langle rr1|e^{i\Delta_2 t} + \text{H.c.}) + V|rr\rangle_{12}\langle rr| \otimes \hat{\mathcal{I}}_3. \tag{12}$$

After moving Eq. (12) to the interaction frame with respect to $\hat{U} \equiv e^{-iV|rr\rangle_{12}\langle rr|\otimes\hat{\mathcal{I}}_3 t}$ and using the condition $\Delta_2 = V$, one can get

$$\hat{H} = \frac{\Omega}{2}(|r11\rangle\langle rr1| + \text{H.c.}). \tag{13}$$

Therefore, $|r11\rangle \rightarrow -i|rr1\rangle$ is achieved after the given π pulse works.

(3) Apply a dispersive π pulse on atom 3 with blue detuning $\Delta_3 = 2V$. In the interaction picture, the Hamiltonian of atom 3 is $\hat{H}_3 = \frac{\Omega}{2}(|1\rangle_3\langle r|e^{i\Delta_3 t} + \text{H.c.})$, and that of the whole system can be written as

$$\begin{aligned}\hat{H} = {} & \frac{\Omega}{2}(|rr1\rangle\langle rrr|e^{i\Delta_3 t} + \text{H.c.}) + V|rr\rangle_{12}\langle rr| \otimes \hat{\mathcal{I}}_3 \\ & + V|rr\rangle_{13}\langle rr| \otimes \hat{\mathcal{I}}_2 + V|rr\rangle_{23}\langle rr| \otimes \hat{\mathcal{I}}_1.\end{aligned} \tag{14}$$

It can be found that $V|rr\rangle_{12}\langle rr| \otimes \hat{\mathcal{I}}_3$ commutes with the other parts of Hamiltonian (14), and thus, its roles in the whole system can be considered independently. Consequently, the phase factor e^{-iVt} is induced in $|rr\rangle_{12}$, which has no influence on the state transfer process. Then, after moving Eq. (14) to the rotating frame with respect to $\hat{U} \equiv e^{-iV(|rr\rangle_{23}\langle rr|\otimes\hat{\mathcal{I}}_1 + |rr\rangle_{13}\langle rr|\otimes\hat{\mathcal{I}}_2)t}$ and substituting the antiblockade condition $\Delta_3 = 2V$, one can get

$$\hat{H} = \frac{\Omega}{2}(|rr1\rangle\langle rrr| + \text{H.c.}), \tag{15}$$

based on which transition $|rr1\rangle \rightarrow -i|rrr\rangle$ is induced after the π pulse.

For the n-qubit ($n > 3$) case, the whole process of RABR can be implemented similarly, which requires n steps and needs, in turn, to manipulate individually the interactions between the laser and Rydberg atom. With the increase in the number of the former excited Rydberg atoms, the energy shift of the latter Rydberg state would be cumulative. Thus, the detuning of the lasers should be manipulated individually to compensate the energy shifts based on the number of the former excited Rydberg atoms.

C. Numerical simulations

In this section, we give the numerical analysis of the present RABR. Suppose the dynamics of the system involving

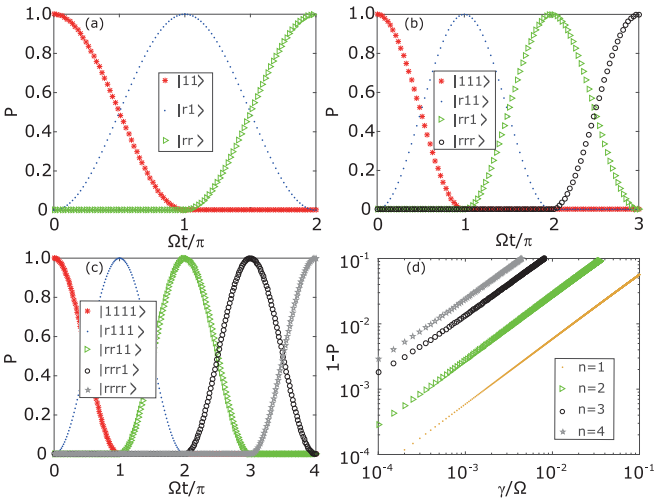

FIG. 3. Variations of populations of relevant states over time for the present (a) two-, (b) three-, and (c) four-qubit RABR schemes, respectively, with γ being set as zero. (d) Populations of collective Rydberg excitation of n-qubit RABR at the proper time versus γ. For the case of $n = 1$, strictly speaking, there is no such thing as the Rydberg blockade and RABR, which require at least two Rydberg atoms. The rest of the parameters are chosen as $\Delta_i = (i-1)V$ and $V = 10\,\Omega$.

decoherence can be described by the Born-Markovian master equation

$$\dot{\hat{\rho}} = -i[\hat{H},\hat{\rho}] + \sum_{i=1}^{n} \frac{\gamma}{2}\mathscr{D}[\hat{\sigma}_i]\hat{\rho}, \tag{16}$$

where $\mathscr{D}[\hat{a}]\hat{\rho} \equiv 2\hat{a}\hat{\rho}\hat{a}^\dagger - \hat{\rho}\hat{a}^\dagger\hat{a} - \hat{a}^\dagger\hat{a}\hat{\rho}$ and $\hat{\sigma}_i = |1\rangle_i\langle r|$ denotes the atomic spontaneous emission process of atom i with rate γ. By solving Eq. (16) numerically via the quantum optics toolbox [42], one can get the dynamical processes of the whole system. As shown in Figs. 3(a)–3(c), we plot the populations of the states participating in the evolution for two-, three-, and four-qubit RABR, respectively, from which one can see the dynamic processes of the RABR. In Fig. 3(d), we plot the populations of collective Rydberg excitation of n-qubit ($n = 2,3,4$) RABR. Since the Rydberg state has a longer lifetime, it is reasonable to suppose γ/Ω is 10^{-3}, and at this point the population of the four-qubit RABR is close to 0.99, and those of the three- and two-qubit cases are higher than 0.99.

IV. APPLICATIONS OF THE PRESENT RABR

A. Controlled-PHASE gates

1. Two-qubit controlled-PHASE gate

As shown in Fig. 4, we consider two Rydberg atoms interacting with each other with the strength V. The transition $|1\rangle_{1(2)} \leftrightarrow |r\rangle_{1(2)}$ is driven resonantly by a π pulse (dispersively with blue detuning Δ by a 2π pulse). The whole process requires three steps.

(1) Applying a resonant π pulse on atom 1, one can get the transitions

$$\{|10\rangle,|11\rangle\} \to -i\{|r0\rangle,|r1\rangle\}. \tag{17}$$

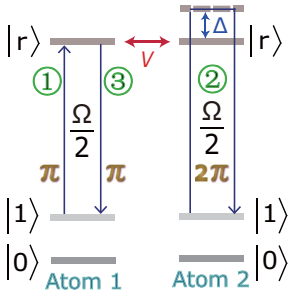

FIG. 4. Illustration of the two-qubit quantum logic gate. Each of the atoms has one Rydberg state $|r\rangle$ and two ground states, $|0\rangle$ and $|1\rangle$. The transition $|1\rangle_{1(2)} \leftrightarrow |r\rangle_{1(2)}$ is driven by a classical laser resonantly (dispersively with blue detuning Δ), in which the subscript i ($i = 1, 2$) means the transition of atom i. The circles with numbers denote the steps.

(2) Apply a dispersive 2π pulse on atom 2. The total Hamiltonian can be divided into two cases according to the initial state of atom 1. In case 1, the initial state of atom 1 is $|0\rangle$. Under the two-atom basis and in the interaction picture, the total Hamiltonian can be rewritten as

$$\hat{H} = \frac{\Omega}{2}(|01\rangle\langle 0r|e^{i\Delta t} + \text{H.c.}). \tag{18}$$

In case 2, the initial state of atom 1 is $|1\rangle$ and has been excited to $|r\rangle$. Similar to Eq. (11), in the interaction picture and rotating the Hamiltonian with respect to the Rydberg interaction term, one can get the total Hamiltonian

$$\hat{H} = \frac{\Omega}{2}(|r1\rangle\langle rr|e^{i(\Delta-V)t} + \text{H.c.}). \tag{19}$$

If the conditions $\Delta = V$ and $\Delta \gg \Omega/2$ are satisfied, the Hamiltonian in Eq. (19) describes a resonant process, while that in Eq. (18) describes a dispersive process with a large detuning and thus can be discarded. Therefore, in this step, one can get the transition

$$|r1\rangle \to -|r1\rangle. \tag{20}$$

(3) Perform a reverse operation of step 1 with a π pulse to return the state of atom 1 to the ground state. Thus, one can get the transitions [43] in this step,

$$\{|r0\rangle,|r1\rangle\} \to i\{|10\rangle,|11\rangle\}. \tag{21}$$

After the three steps described above, the whole transitions can be illustrated as

$$\begin{bmatrix} 1 & 0 & 0 & 0 \\ 0 & 1 & 0 & 0 \\ 0 & 0 & 1 & 0 \\ 0 & 0 & 0 & -1 \end{bmatrix} \tag{22}$$

in the basis $\{|00\rangle,|01\rangle,|10\rangle,|11\rangle\}$, which is the standard two-qubit quantum controlled-PHASE gate. The total required time for this scheme is $t = 4\pi/\Omega$.

2. Multiqubit controlled-PHASE gate

We now show how the RABR-based multiqubit quantum controlled-PHASE gate works. We first consider the case where the atoms are trapped in a two-dimensional (2D) optical lattice

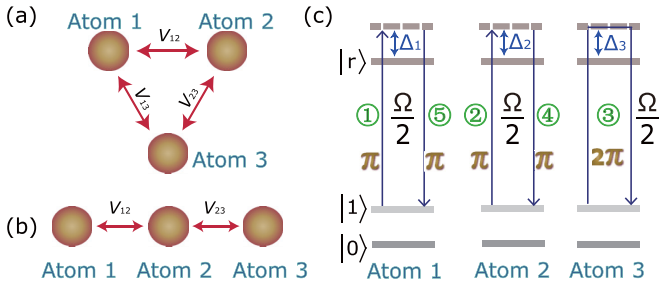

FIG. 5. (a) Three interacting Rydberg atoms in a 2D optical lattice. (b) Three Rydberg atoms with nearest-neighboring interaction in a 1D optical lattice. (c) Illustration of a three-qubit controlled PHASE gate. In order to facilitate the analysis and design, we let the RRI strength $V_{12} = V_{23} = V_{13} = V$. Δ_s denotes the detuning between atom s and the corresponding transition $|1\rangle_s \to |r\rangle_s$. The antiblockade conditions for (a) and (b) are $\Delta_s = (s-1)V(s = 1,2,3)$ and $\Delta_s = V(s \neq 1)$ and $\Delta_s = 0(s = 1)$, respectively.

and every pair has RRI. As shown in Fig. 5(a), the whole process requires five steps.

(1) Apply a resonant π pulse on atom 1. One can get the transitions

$$\{|100\rangle,|101\rangle,|110\rangle,|111\rangle\} \to -i\{|r00\rangle,|r01\rangle,|r10\rangle,|r11\rangle\}. \tag{23}$$

(2) Apply a dispersive π pulse on atom 2 with blue detuning Δ_2. Thus, the Hamiltonian of atom 2 is $\hat{H}_2 = \frac{\Omega}{2}(|1\rangle_2\langle r|e^{i\Delta_2 t} + \text{H.c.})$, and that of the whole system can be expressed as

$$\hat{H} = \frac{\Omega}{2}[(|r11\rangle\langle rr1| + |r10\rangle\langle rr0|)e^{i\Delta_2 t} + \text{H.c.}] + V|rr\rangle_{12}\langle rr| \otimes \hat{\mathcal{I}}_3 \tag{24}$$

or

$$\hat{H} = \frac{\Omega}{2}[(|011\rangle\langle 0r1| + |010\rangle\langle 0r0|)e^{i\Delta_2 t} + \text{H.c.}], \tag{25}$$

depending on whether the initial state of the first Rydberg atom is $|1\rangle$ or $|0\rangle$. By moving to the rotating frame and substituting the condition $\Delta_2 = V$, one can simplify Eq. (24) to

$$\hat{H} = \frac{\Omega}{2}(|r11\rangle\langle rr1| + |r10\rangle\langle rr0| + \text{H.c.}). \tag{26}$$

In contrast to Eq. (26), Eq. (25) describes the dispersive interactions with detuning $\Delta_2 \gg \Omega/2$ and thus can be discarded safely. Accordingly, the evolution process of this step is

$$\{|r10\rangle,|r11\rangle\} \to -i\{|rr0\rangle,rr1\rangle\}. \tag{27}$$

(3) Apply a dispersive 2π pulse on atom 3 with blue detuning $\Delta_3 = 2V$. In the interaction picture, the Hamiltonian of atom 3 is $\hat{H}_3 = \frac{\Omega}{2}(|1\rangle_3\langle r|e^{i\Delta_3 t} + \text{H.c.})$, and that of the whole system can be classified as the following cases based on the states of the former two atoms. In case 1,

$$\hat{H} = \frac{\Omega}{2}[(|001\rangle\langle 00r| + |011\rangle\langle 01r|)e^{i\Delta_3 t} + \text{H.c.}], \tag{28}$$

which describes a dispersive interaction with detuning Δ_3. In case 2,

$$\hat{H} = \frac{\Omega}{2}(|r01\rangle\langle r0r|e^{i\Delta_3 t} + \text{H.c.}) + V|rr\rangle_{13}\langle rr| \otimes \hat{\mathcal{I}}_2, \tag{29}$$

which also describes a dispersive interaction between $|r01\rangle$ and $|r0r\rangle$ with detuning $\Delta_3 - V$. In case 3,

$$\hat{H} = \frac{\Omega}{2}(|rr1\rangle\langle rrr|e^{i\Delta_3 t} + \text{H.c.}) + V|rr\rangle_{12}\langle rr| \otimes \hat{\mathcal{I}}_3 + V|rr\rangle_{13}\langle rr| \otimes \hat{\mathcal{I}}_2 + V|rr\rangle_{23}\langle rr| \otimes \hat{\mathcal{I}}_1, \tag{30}$$

which is simplified to

$$\hat{H} = \frac{\Omega}{2}(|rr1\rangle\langle rrr| + \text{H.c.}) + V|rr\rangle_{12}\langle rr| \otimes \hat{\mathcal{I}}_3 \tag{31}$$

after moving it to the rotating frame with respect to $\hat{U} \equiv e^{-iV(|rr\rangle_{23}\langle rr|\otimes\hat{\mathcal{I}}_1 + |rr\rangle_{13}\langle rr|\otimes\hat{\mathcal{I}}_2)t}$ and substituting the antiblockade condition $\Delta_3 = 2V$. Equation (31) describes a resonant interaction between $|rr1\rangle$ and $|rrr\rangle$, and $V|rr\rangle_{12}\langle rr| \otimes \hat{\mathcal{I}}_3$ will induce a phase factor e^{-iVt_1} ($t_1 = 2\pi/\Omega$ for a 2π pulse) on state $|rr\rangle_{12}$ regardless of the state of atom 3. In contrast to case 3, cases 1 and 2 can be discarded safely since they describe dispersive interactions. Thus, the transitions corresponding to this step are

$$\{|rr0\rangle,|rr1\rangle\} \to e^{-iVt_1}\{|rr0\rangle, -|rr1\rangle\}. \tag{32}$$

(4) This step is the reverse process of step 2 with the pulse having a π relative phase.

(5) This step is the reverse process of step 1 with the pulse having a π relative phase.

After the five steps described above, the whole evolution process is

$$\begin{aligned} &|000\rangle \to |000\rangle, \quad |001\rangle \to |001\rangle, \quad |010\rangle \to |010\rangle, \\ &|011\rangle \to |011\rangle, \quad |100\rangle \to |100\rangle, \quad |101\rangle \to |101\rangle, \\ &|110\rangle \to e^{-iVt_1}|110\rangle, \quad |111\rangle \to -e^{-iVt_1}|111\rangle. \end{aligned} \tag{33}$$

If $Vt_1 = 2n\pi$ ($n \in$ integrals and $n \neq 0$), which can be fulfilled by adjusting $V = n\Omega$, the desired three-qubit controlled-PHASE gate is achieved.

For the n-qubit ($n > 3$) case, C_n^2 Rydberg interactions exist. In order to facilitate the analysis, we let all of the RRI strengths equal V. The whole process of the n-qubit controlled-PHASE gate requires $2n-1$ steps. The physical process to realize the n-qubit controlled-PHASE gate comes from that to realize the RABR. On the premise that the Rydberg antiblockade condition is fulfilled, one should apply π pulses to excite the former $n-1$ atoms sequentially. Then, a 2π pulse should be applied on the nth atom, and the π phase would emerge or not based on the state of the former atoms. The next step is to perform reverse operations to return the former $n-1$ atoms to the ground state sequentially. It is worth specially mentioning that the additional phase e^{-iVt} would be induced for the states with two Rydberg excitations. However, as mentioned above, this undesirable phase can be eliminated by adjusting the ratio between V and Ω. The total time for the RABR-based n-qubit quantum logic gate is $t = 2n\pi/\Omega$, which is the same as the sequentially addressed and blockade-based one in Ref. [30]. [In fact, the scheme in Ref. [30] is to construct the C_n-NOT

gate, and the required time is $(2n+3)\pi/\Omega$. If the scheme is used for the controlled-PHASE gate, the required time is the same as the current one.]

For the Rydberg atoms with near-neighbor interactions, as shown in Fig. 5(b), the RABR and the corresponding logic gate can also be implemented by modifying the antiblockade condition as $\Delta_s = V(s \neq 1), \Delta_s = 0(s = 1)$. Thus, the latter Rydberg atom in state $|1\rangle$ is excited or not depending on the state of the previous nearest-neighbor atom, and the conditional dynamics is achieved. In addition to the detunings being different, the steps and the shapes of the pulses of Fig. 5(b) are the same as those of Fig. 5(a).

3. *Numerical simulations*

We now give numerical analysis about the present RABR-based logic gates. The evolution of the whole system is governed by the master equation

$$\dot{\hat{\rho}} = -i[\hat{H}, \hat{\rho}] + \sum_{i=1}^{n} \sum_{j=0}^{1} \mathscr{D}[\hat{\sigma}_{i,j}]\hat{\rho}, \tag{34}$$

in which $\mathscr{D}[\hat{a}]\hat{\rho} \equiv \hat{a}\hat{\rho}\hat{a}^\dagger - (\hat{\rho}\hat{a}^\dagger\hat{a} + \hat{a}^\dagger\hat{a}\hat{\rho})/2$ and $\hat{\sigma}_{i,j} = \sqrt{\gamma/2}|j\rangle_i\langle r|$ denotes the atomic spontaneous emission process from $|r\rangle$ to $|j\rangle$ of atom i with the equational rate $\gamma/2$ for the two ground states. In the strict sense, using only one group of specific initial state is insufficient to test the performance of the logic gate. One way is to use the trace-preserving quantum-operator-based (TPQO) average fidelity defined as [44,45]

$$\overline{F}(\hat{\mathcal{O}}, \varepsilon) = \frac{\sum_j \mathrm{tr}[\hat{\mathcal{O}}\hat{\mathcal{O}}_j^\dagger \hat{\mathcal{O}}^\dagger \varepsilon(\hat{\mathcal{O}}_j)] + d^2}{d^2(d+1)}, \tag{35}$$

in which $\hat{\mathcal{O}}_j$ is the tensor of Pauli matrices $\hat{I}\hat{I}, \hat{I}\hat{\sigma}_x, \ldots, \hat{\sigma}_z\hat{\sigma}_z (\hat{I}\hat{I}\hat{I}, \hat{I}\hat{I}\hat{\sigma}_x, \ldots, \hat{\sigma}_z\hat{\sigma}_z\hat{\sigma}_z)$ for two(three)-qubit quantum logic gate, $\hat{\mathcal{O}}$ is the perfect phase gate, ε is the trace-preserving quantum operation obtained with the present logic gate, and $d = 2^n$ for n-qubit quantum logic gate. One can also use several groups of random initial states (RIS) to accomplish this goal. The weighted average of the fidelities, $\bar{F} = (\sum_{s=1}^{n} {}_s\langle\psi|\hat{\rho}|\psi\rangle_s)/n$, with $|\psi\rangle_s$ being the sth ideal final state originating from the ideal quantum controlled-PHASE gate and the sth random initial state and $\hat{\rho}$ being the practical final state from the master-equation method, is another way to measure the average fidelity.

By solving the master equations numerically, we show the temporal evolution of the average fidelity of two- and three-qubit quantum logic gates including the final step in Fig. 6(a), with the RIS and TPQO methods, respectively. Figure 6(b) shows the variances with respect to γ at the optimal time. Since the Rydberg state has a long lifetime, the schemes can have a better performance and certain robustness on decoherence of spontaneous emission.

B. Rydberg excitation superatom

1. *Fundamentals*

A "Rydberg superatom"(RSA) is essentially an ensemble composed of N Rydberg atoms excited by light to the Rydberg state, where the dipole blockade mechanism allows only a single collective excitation in the whole ensemble, thus forming

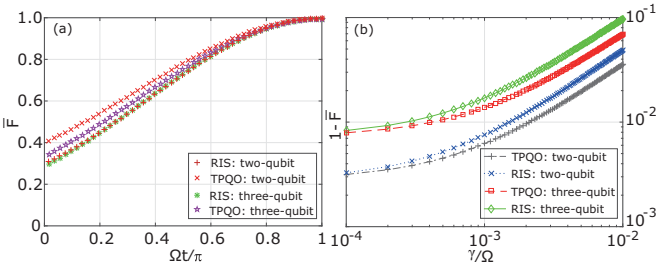

FIG. 6. (a) Average fidelity of the final step of two- and three-qubit controlled-PHASE gates, with the RIS method and the TPQO method. The parameters are set as $V = 12\,\Omega, \Delta = V$ and $\gamma = 0$. We have reset the initial time of the final step to be zero for clarity. (b) Average fidelity with respect to γ at the optimal time for two- and three-qubit cases under the RIS and TPQO methods. The parameters are set as $V = 12\,\Omega, \Delta_i = (i-1)V$. For the RIS method, we use 1000 (500) groups of random initial states to test the performance of a two- (three-) qubit logic gate.

an effective two-level system [4] whose effective ground state and excited state are the collective ground state and Dicke state of the ensemble, respectively. In this regime, the RSA leads to an enhanced atom-light coupling strength of $\sqrt{N}$ [4].

Unlike the RSA model that can enhance the coupling strength, we propose a scheme to construct the "Rydberg excitation superatom"(RESA) model, which can (i) decrease the blockade error, (ii) enlarge the blockade radius, and (iii) also be feasible in the intermediate RRI strength for the blockade-based schemes based on the present RABR that allows more than one atom to be excited to the Rydberg state in a short time. The RESA model is composed of at least two Rydberg atoms and requires collectively encoding the Rydberg atoms as $|\bar{0}\rangle \equiv |00\cdots\rangle, |\bar{1}\rangle \equiv |11\cdots\rangle, |\bar{r}\rangle \equiv |rr\cdots\rangle$.

2. *Controlled-PHASE gate with RESA*

For simplicity, as shown in the shaded area in Fig. 7(a), we first consider the RESA by pairing qubits as the logic qubit and using it to construct the blockade controlled-PHASE gate. The blockade controlled-PHASE gate was first introduced by Jaksch *et al.* [3] and was widely studied in theory [2]

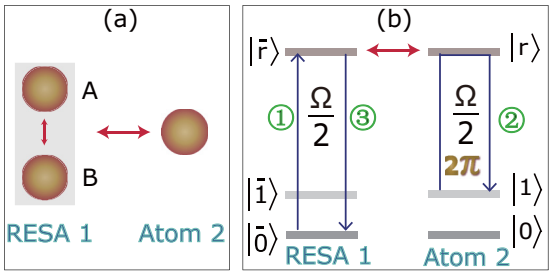

FIG. 7. Controlled-PHASE gate based on the RESA. (a) RESA interacting with a Rydberg atom. The logic qubits of the RESA are $\{|\bar{0}\rangle \equiv |00\rangle_{AB}, |\bar{1}\rangle \equiv |11\rangle_{AB}\}$. (b) The process to realize the RESA-based Rydberg blockade controlled-PHASE gate. Quantum information of the RESA is stored in the basis states $|\bar{0}\rangle$, $|\bar{1}\rangle$. Ω is the Rabi frequency between the corresponding ground state and Rydberg state.

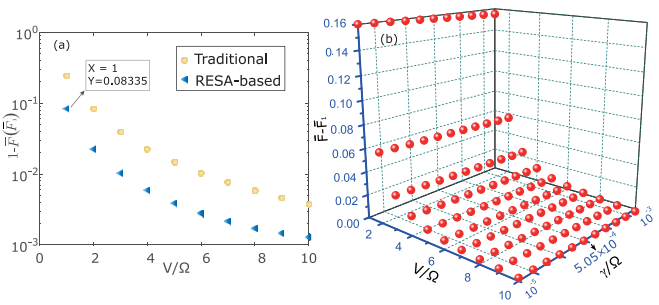

FIG. 8. (a) Average fidelity $\bar{F}$ ($\bar{F}_1$) of the RESA-based (traditional) blockade two-qubit controlled-PHASE gate. (b) $\bar{F} - \bar{F}_1$ versus V and γ.

and verified in experiment [19]. The performance of the gate after applying the RESA was investigated. The whole process requires three steps:

(1) Apply the RABR pulses on RESA 1 to realize $|\bar{0}\rangle \rightarrow |\bar{r}\rangle$, similar to the process in Sec. III A.

(2) Apply a 2π pulse on target atom 2 to realize $|1\rangle \rightarrow -|1\rangle$.

(3) Perform the reverse operation of step 1 to return to the state of RESA 1.

3. *Performance and discussion*

By solving the master equation numerically, as shown in Fig. 8, we make a comparison between the RESA-based two-qubit controlled-PHASE gate and the traditional one. From Fig. 8(a), one can see that in the intermediate RRI strength, $V \sim \Omega$, $\bar{F}$ is still higher than 91.6%. Figure 8(b) shows the difference between $\bar{F}$ and $\bar{F}_1$ versus V and γ. It is shown that the difference decreases noticeably as V increases but slowly as γ increases. That is, the feature of the RESA-based scheme is more obvious in the intermediate- and near-intermediate-RRI-strength regions than that in the strong-RRI regions. And the scheme has almost the same robustness as the traditional one on atomic spontaneous emission. Although the process to achieve the logic gate does not require the possibility of arbitrary single-logic-qubit operations on RESA, more complex quantum information processing tasks based on RESA may require it. As pointed out in Ref. [31], the arbitrary single-logic-qubit operations can be decomposed as a product of rotations $\{\bar{U}(\beta)|\bar{0}\rangle = \cos\frac{\gamma}{2}|\bar{0}\rangle + \sin\frac{\gamma}{2}|\bar{1}\rangle, \bar{U}(\beta)|\bar{1}\rangle = \cos\frac{\gamma}{2}|\bar{0}\rangle - \sin\frac{\gamma}{2}|\bar{1}\rangle\}$ and a gate which can be understood as a rotation about the z axis $\{\bar{U}_z(\alpha)|\bar{0}\rangle = e^{-i\alpha}|\bar{0}\rangle, \bar{U}_z(\alpha)|\bar{1}\rangle = e^{i\alpha}|\bar{1}\rangle\}$. $\bar{U}(\beta)$ can be realized as $\bar{U}(\beta) = \mathrm{C}_{\mathrm{NOT}}^{\mathrm{A,B}} U^A(\beta) \mathrm{C}_{\mathrm{NOT}}^{\mathrm{A,B}}$, where $\mathrm{C}_{\mathrm{NOT}}^{\mathrm{A,B}}$ denotes a controlled-NOT gate with atoms A and B being the control and target qubits, respectively. $\bar{U}_z$ can be constructed as $\bar{U}_z = U_z^A \otimes I^B$.

In the former paragraph, we compare only the RESA-based blockade two-qubit quantum logic gate with the traditional one. Almost all previous blockade-based quantum information processing tasks can be reevaluated with the introduction of RESA. Moreover, the case for mutiatom-formed RESA can also be studied in a similar way. Nevertheless, we should be aware that as the number of atoms in RESA increases, the robustness of the scheme to decoherence inevitably decreases.

V. DISCUSSION

A. Some practical considerations

The RABR and the corresponding logic gate are influenced mainly by the factors, namely, uncertainty in the atomic separation [46], two-body forces, and ionization [47–51]. Li *et al.* [46] showed that the mechanical effect among the Rydberg atoms as well as the spread of the atomic packet can affect the excitation dynamics in the RABR with simultaneous driving. The regimes with $r_0/\Delta r$ (r_0 is the initial distance between Rydberg atoms, and Δr is the uncertainty in the atomic separation) equal to 72 and 30 show strikingly different character on the Rabi oscillation between the collective ground state $|gg\rangle$ and the Rydberg state $|ee\rangle$. The former regime shows better coherence than the latter one. One of the causes of this case is the needless and inevitable laser-driven coupling among the motion states within an energy window $\sim F\Delta r$ [46], where $F = -\partial_r V(r)|_{r=r_0}$ denotes the force between the Rydberg atoms at distance r_0. Thus, the distance between the atoms determines the force and further influences the excitation of the motion state. For the present two-qubit RABR with sequent driving, the conditions become more relaxed since the required time involved in the whole process is far less than that of the one with simultaneous driving. For a rough estimation, we suppose the force F is constant in the whole RABR process (in fact, during the excitation process the force is far less than F) and the two RABRs have the same momentum transfer on the atoms. The required time of the present RABR is $2\pi/\Omega$, and that of the simultaneous driving one is $\pi\Delta/\Omega^2$. If we set $\Delta = 10\,\Omega$, the coherence of the present RABR can be preserved to a large extent if the force increases (the maximum is up to 5 times). Thus, if we consider the RRI strength proportionate to C_6/r_6, $r_0/\Delta r \simeq 55.1$ can be estimated to preserve quantum coherence for the present two-qubit RABR.

Other situations should be considered for the multiqubit quantum logic gate since the mechanical effect will have more influence, including motional heating [47] and ionization [49–51], when two or more atoms are excited to the Rydberg state. As pointed out in Ref. [47], the peak heating rate can be estimated simply as $P = Fv \sim m\hbar V\tilde{v}/r$, where m is determined by the RRI form and $\tilde{v}$ is influenced by the laser. This method is applied to estimate the performance of the classic Rydberg-atom-based quantum logic scheme [47], model A in Ref. [3], in which the authors get $P \sim 1.8\ \mu\mathrm{K}/\mu\mathrm{s}$, with $V = 2\pi \times 1$ MHz, $r = 50\ \mu$m, and the other rational laser parameters. The radial vibrational state space in temperature units is $\Delta E_{\mathrm{vib}} = \hbar\omega/k_B = 1.9\ \mu$K. The required time is $2\pi/\Omega + \pi/V > 0.5\ \mu$s, with the condition $\Omega \gg V$, and thus, the peak heating value is comparable to ΔE_{vib}. Because the atoms spend proportionately more time near the turning points of the motion, the probability of a change in the vibrational state can be well reduced [47]. For the present three-qubit quantum logic gate, the condition $V \gg \Omega$ is satisfied, and the duration time for at least two atoms on Rydberg state is $2\pi/\Omega$. On the one hand, one can enhance the Rabi frequency of the laser to reduce the required time. On the other hand, large Ω requires even greater V to fulfill the condition $V \gg \Omega$, which would enhance F and the heating rate. If we choose $V = 2\pi \times 10$ MHz and $\Omega = 2\pi \times 5$ MHz and suppose the other conditions remain invariant, the system will have a little stronger

heating effect than the one in Refs. [3,47]. However, this situation can be improved a little bit by enlarging r appropriately.

Another situation that should be discussed is the ionization [49–51] when two or more atoms are on the Rydberg state and exhibit attractive [50] or repulsive [51] interactions. Ionization occurs when both of the excited atoms accelerate toward each other and collide. In Ref. [50], by using penning ionization on a microsecond time scale as a probe, researchers gave an effective way to reveal the pair dynamics for excited atomic gas in the presence of the attractive two-body forces. Two main conclusions were drawn by analyzing the shift of the ionization line: (i) For a short interaction time, only very close atom pairs, which are preferentially excited at large detuning, can collide, and the ion signal is weak. (ii) For very long times, the ion signal is strong, and almost all atoms are ionized. In other words, the time when both Rydberg atoms are in the excited state and the distance between the excited atoms are two factors that influence the ionization. In addition, the repulse interaction can also induce the ionization, which is discussed in Ref. [51]. For more than 1000 Rydberg atoms in the excitation volume, one can see from Fig. 3 of Ref. [50] that the fraction of ionized atoms is close to zero when the excitation time is less than 2.1 μs and the relevant Rydberg state is the 60S state. For our three-qubit scheme, when we choose $V = 2\pi \times 30$ MHz, $\Omega = 2\pi \times 5$ MHz, the time when the first two atoms are in the excited state is $2\pi/\Omega = 0.2\,\mu$s, which is far less than the ionization time. Thus, the ionization rate can be ignored, at least in theory, for schemes with a qubit number less than 10. And the 60S state can thus be considered the Rydberg energy level for our multiqubit schemes. In addition, from the above analysis, one can see that although the higher principal quantum number can increase the interaction strength V and lifetime to enable larger Rabi frequency and fast operations, the strong mechanical effect and the ionization would be induced as V increases. That is the reason why we cannot choose a higher principal quantum number.

The ionization and other mechanical effects can be minimized by changing some of the steps of the quantum logic gate. The main physical thought of this improvement is to reduce the time when two or more atoms are in the Rydberg state simultaneously to zero. For simplicity, we take the three-qubit case as an example. We keep steps 1 and 2 the same as those in Sec. IV A 2.

(3) Apply a π pulse on atom 1 with detuning $\Delta = V$ and a π phase relative to step 1, which induces the evolutions $\{|rr0\rangle, |rr1\rangle\} \rightarrow i\{|1r0\rangle, |1r1\rangle\}$.

(4) Apply a π pulse on atom 1 resonantly with the π phase relative to step 1. The corresponding evolutions are $\{|r00\rangle, |r01\rangle\} \rightarrow i\{|100\rangle, |101\rangle\}$.

(5) Apply a 2π pulse on atom 3 with detuning $\Delta = V$. The corresponding evolution is $|1r1\rangle \rightarrow -|1r1\rangle$.

(6) Apply a π pulse on atom 1 resonantly. The evolutions of this step are $\{|100\rangle, |101\rangle\} \rightarrow -i\{|r00\rangle, |r01\rangle\}$.

(7) Apply a π pulse on atom 1 with detuning $\Delta = V$. The corresponding evolutions are $\{|1r0\rangle, |1r1\rangle\} \rightarrow -i\{|rr0\rangle, |rr1\rangle\}$.

(8) Apply a π pulse on atom 2 with detuning $\Delta = V$ and a π phase relative to step 2. The evolutions $\{|rr0\rangle, |rr1\rangle\} \rightarrow i\{|r10\rangle, |r11\rangle\}$ are achieved.

TABLE I. Partial experimental parameters used in Ref. [52].

Experimental parameter	Symbol	Value
Rydberg level	$\|r\rangle$	$97d_{5/2}$
Rydberg state radiative lifetime	τ	320 μs
Blockade shift	V	$2\pi \times 20$ MHz
Rydberg red Rabi frequency	Ω_R	$2\pi \times 118$ MHz
Rydberg blue Rabi frequency	Ω_B	$2\pi \times 39$ MHz
Rydberg red detuning	Δ_{p1}, Δ_{p2}	$2\pi \times 2$ GHz
Rydberg Rabi frequency	Ω	$2\pi \times 1.15$ MHz

(9) Apply a π pulse on atom 1 resonantly with the π phase relative to step 1. The evolutions of this step are $\{|r00\rangle, |r01\rangle, |r10\rangle, |r11\rangle\} \rightarrow i\{|100\rangle, |101\rangle, |110\rangle, |111\rangle\}$.

After the whole process, $|111\rangle \rightarrow -|111\rangle$ is achieved while other states remain invariant. During the whole process, the time when two atoms are in Rydberg states is at the end of step 7 or at the beginning of step 8. The period of time can thus be considered zero. Thus, the additional phase e^{-iVt} is eliminated, and the condition for a multiqubit controlled-PHASE gate, $V = n\Omega (n \in \text{Integer})$, is no longer needed. The numerical simulation with $V = 20.2\,\Omega$ shows the fidelity of this modified scheme can be 0.992.

B. Numerical simulations with experimental parameters

In this section, we use one group of typical experimental parameters extracted from Ref. [52], as shown in Table. I, to discuss the feasibility and the robustness on parameter fluctuation. The decay rate γ is inversely proportional to the lifetime τ: $\gamma \simeq 1/\tau = 3.125$ kHz. In Ref. [52], researchers used the ground hyperfine states $|5s_{1/2}, f = 1, m_f = 0\rangle$ and $|5s_{1/2}, f = 2, m_f = 0\rangle$ to encode qubits $|0\rangle$ and $|1\rangle$, respectively. To realize the effective coupling $|1\rangle \rightarrow |r\rangle \equiv |97d_{5/2}, m_j = 5/2\rangle$ and the single-qubit rotations $|0\rangle \leftrightarrow |1\rangle$, the intermediate state $|p\rangle \equiv |5p_{3/2}, f' = 2\rangle$ is introduced. The Rabi frequencies of $|1\rangle \rightarrow |p\rangle$ and $|p\rangle \rightarrow |r\rangle$ are Ω_B and Ω_R, respectively. Suppose the detunings of these two transitions are Δ_{p1} and $-\Delta_{p2}$, respectively. Thus, the effective Rabi frequency and detuning of $|1\rangle \rightarrow |r\rangle$ are $\Omega \simeq \Omega_R \Omega_B / 2\bar{\Delta}$, with $\bar{\Delta} = 2\Delta_{p1}\Delta_{p2}/(\Delta_{p1} + \Delta_{p2})$, and $\Delta_{p2} - \Delta_{p1}$, respectively. In the experiment they set $\Delta_{p1} = \Delta_{p2} = \Delta_p$, and thus, $\Omega \simeq 2\pi \times 1.15$ MHz and $\Delta = 0$ are achieved. However, in our scheme, different detunings for different atoms are required. One way to accomplish this is to adjust the difference between Δ_{p1} and Δ_{p2}. In spite of that, the requirement and process of the present RABR-based two-qubit quantum logic gate are almost the same as that in Ref. [52]. Thus, we have reason to believe that the experimental parameters can be used in our scheme. The Rydberg level $97d_{5/2}$ is also valid for the RABR-based two-qubit scheme. In the following we consider only the two-qubit case for simplicity. Figure 9(a) shows that the fidelity is close to 0.999 when the spontaneous emission rate is about 1 kHz. For the experimental parameter $\gamma = 3.125$ kHz, the fidelity is still close to 0.997.

In addition, fluctuations of Ω and V are induced due to the noise, atomic movement, and other operation imperfections. To see its effect on the average fidelity clearly, we suppose the fluctuation of parameter ϵ ($\epsilon = \Omega$ or V) satisfying the

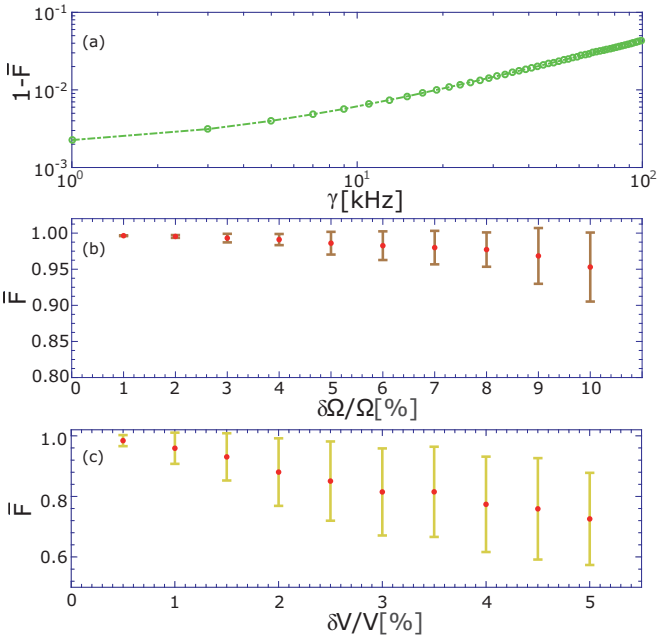

FIG. 9. Performance of the two-qubit controlled-PHASE gate with the parameters extracted from experiment [52]. (a) Average fidelity versus γ at time $4\pi/\Omega$. The relevant parameters are taken from Table I. The mean maximal fidelities versus scaled standard deviations of inhomogeneous parameters (b) Ω and (c) V. The error bars show the standard deviation of $\{F^j_{\max}\}$. The rest of the parameters in (b) and (c) are the same as in (a), and the TPQO method defined in Eq. (35) is used.

Gaussian distribution with mean ϵ_0 and standard deviation $\delta\epsilon$. For a sample array $\{\epsilon_j\}$, we calculate the maximal fidelity in a single evolution. For a fixed $\delta\epsilon$, the mean value of the maximal fidelity is calculated as $\overline{F} = (\sum_1^m F^j_{\max})/m$, in which m is the time of the single evolution. Accordingly, the standard deviation of $F^j_{\max}$ is also calculated. In Figs. 9(b) and 9(c), we plot the variations of the mean maximal fidelity versus $\delta\Omega/\Omega$ and $\delta V/V$, respectively, with $m = 200$, which show that the fidelity is more sensitive to the fluctuation of V than to that of Ω since the condition of RABR would be broken if V were to fluctuate. Experimentally, one can decrease this effect in two ways. One is to reduce the gate time by enhancing the value of Ω since any detrimental influence can be reduced as the interaction time decreases. The other is to lower the temperature of single atoms [53]. Another point worth noting is that the present schemes require individual addressing of atoms, which is a relatively mature technique with current technology [19,52,53].

For the multiqubit case, the scheme does not require the RRI strengths V_{ij} between any two atoms to be equal. In this case, the RABR condition can also be met by adjusting the corresponding detunings. Also, the scheme can work under strong or weak RRI strength on the premise that the antiblockade condition is satisfied.

C. Influence of dephasing error

Compared to the lower atomic spontaneous emission rate, Rydberg atoms have another lager dissipation factor,

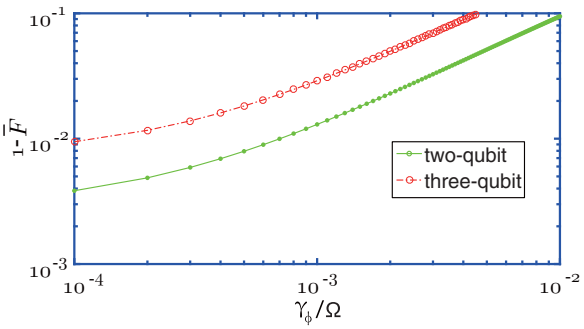

FIG. 10. Performance of the RABR-based two- and three-qubit controlled-PHASE gates with dephasing error.

i.e., dephasing error. The Lindblad operator describing the dephasing of atom j can be written as $\hat{L}_j = \sqrt{\gamma_\phi}(|1\rangle_j\langle 1| + |0\rangle_j\langle 0| - |r\rangle_j\langle r|)$ or $\hat{L}_j = \sqrt{\gamma_\phi}(\hat{\mathcal{I}}_j - 2|r\rangle_j\langle r|)$ [25]. We use the master-equation method to qualify its influence on our schemes, as shown in Fig. 10. After making a comparison between Figs. 10 and 6(b), one can see that the dephasing has a slightly greater influence than atomic spontaneous emission on the system. This situation becomes apparent when the dephasing rate becomes larger than the atomic spontaneous emission rate. One of the effective ways to decrease this influence is to decrease the operation time of the system if the condition allows.

D. Possible extensions of the application

The physical thought of the present RABR is feasible not only for the Rydberg atom but also for the other models which have near-neighbor interactions. Also, the present RABR can further be used to research the motional effects for Rydberg atoms using the method in Refs. [46,54] and provides an alternative excitation method for researching the ionization [47–51] in a more efficient manner since the present RABR is fast. Furthermore, the present antiblockade regime is also valid for Rydberg ensembles (Rydberg superatoms) and can be used to construct the quantum logic gate for RSA. On the other hand, if one knows the precise effective distance between Rydberg ensembles, some Rydberg-superatom-based quantum information operations can be implemented accurately. For the regular-arrangement-atom-constructed ensembles, one can use the distance between the central atoms of each ensemble to estimate the effective distance. However, things become tricky for the irregular-arrangement-atom-constructed ensembles. With the present RABR, the effective distance between Rydberg ensembles can be measured precisely. One can excite one of the RSA first and scan the absorption spectra on the second RSA. The peak value of the absorption spectra reveals the RRI strength between two Rydberg ensembles and further displays the information about the distance.

VI. CONCLUSION

In conclusion, we proposed an alternative scheme to realize RABR in a short period of time, which, unlike most of the current schemes, allows more than two Rydberg atoms to be excited. The two- and multiqubit controlled-PHASE gates

were constructed based on the present RABR. Then the RABR-based RESA model with little blockade error and large blockade radius was presented and studied. Discussions on the mechanical effect, ionization, and simulations with experimental parameters showed the scheme can be performed robustly. In addition, other possible applications of the present RABR were also discussed.

ACKNOWLEDGMENTS

This work was supported by the Young Teacher Start-up Foundation of Zhengzhou University, National Natural Science Foundation of China, under Grants No. 61465013 and No. 11404290 and the Natural Science Foundation of the Henan Educational Committee (17A140002).

[1] T. F. Gallagher, *Rydberg Atoms* (Cambridge University Press, Cambridge, 1994).

[2] M. Saffman, T. G. Walker, and K. Mølmer, Quantum information with Rydberg atoms, Rev. Mod. Phys. **82**, 2313 (2010).

[3] D. Jaksch, J. I. Cirac, P. Zoller, S. L. Rolston, R. Côté, and M. D. Lukin, Fast Quantum Gates for Neutral Atoms, Phys. Rev. Lett. **85**, 2208 (2000).

[4] M. D. Lukin, M. Fleischhauer, R. Cote, L. M. Duan, D. Jaksch, J. I. Cirac, and P. Zoller, Dipole Blockade and Quantum Information Processing in Mesoscopic Atomic Ensembles, Phys. Rev. Lett. **87**, 037901 (2001).

[5] D. Tong, S. M. Farooqi, J. Stanojevic, S. Krishnan, Y. P. Zhang, R. Côté, E. E. Eyler, and P. L. Gould, Local Blockade of Rydberg Excitation in an Ultracold Gas, Phys. Rev. Lett. **93**, 063001 (2004).

[6] K. Singer, M. Reetz-Lamour, T. Amthor, L. Gustavo Marcassa, and M. Weidemüller, Suppression of Excitation and Spectral Broadening Induced by Interactions in a Cold Gas of Rydberg Atoms, Phys. Rev. Lett. **93**, 163001 (2004)

[7] T. Cubel Liebisch, A. Reinhard, P. R. Berman, and G. Raithel, Atom Counting Statistics in Ensembles of Interacting Rydberg Atoms, Phys. Rev. Lett. **95**, 253002 (2005).

[8] R. Heidemann, U. Raitzsch, V. Bendkowsky, B. Butscher, R. Löw, L. Santos, and T. Pfau, Evidence for Coherent Collective Rydberg Excitation in the Strong Blockade Regime, Phys. Rev. Lett. **99**, 163601 (2007).

[9] E. Urban, T. A. Johnson, T. Henage, L. Isenhower, D. D. Yavuz, T. G. Walker, and M. Saffman, Observation of Rydberg blockade between two atoms, Nat. Phys. **5**, 110 (2009).

[10] A. Gaëtan, Y. Miroshnychenko, T. Wilk, A. Chotia, M. Viteau, D. Comparat, P. Pillet, A. Browaeys, and P. Grangier, Observation of collective excitation of two individual atoms in the Rydberg blockade regime, Nat. Phys. **5**, 115 (2009).

[11] T. Wilk, A. Gaëtan, C. Evellin, J. Wolters, Y. Miroshnychenko, P. Grangier, and A. Browaeys, Entanglement of Two Individual Neutral Atoms Using Rydberg Blockade, Phys. Rev. Lett. **104**, 010502 (2010).

[12] J. D. Pritchard, D. Maxwell, A. Gauguet, K. J. Weatherill, M. P. A. Jones, and C. S. Adams, Cooperative Atom-Light Interaction in a Blockaded Rydberg Ensemble, Phys. Rev. Lett. **105**, 193603 (2010).

[13] Y. O. Dudin and A. Kuzmich, Strongly interacting Rydberg excitations of a cold atomic gas, Science **336**, 887 (2012).

[14] Y. O. Dudin, L. Li, F. Bariani, and A. Kuzmich, Observation of coherent many-body Rabi oscillations, Nat. Phys. **8**, 790 (2012).

[15] P. Schauß, M. Cheneau, M. Endres, T. Fukuhara, S. Hild, A. Omran, T. Pohl, C. Gross, S. Kuhr, and I. Bloch, Observation of spatially ordered structures in a two-dimensional Rydberg gas, Nature (London) **491**, 87 (2012).

[16] G. Günter, H. Schempp, M. Robert-de-Saint-Vincent, V. Gavryusev, S. Helmrich, C. S. Hofmann, S. Whitlock, and M. Weidemuller, Observing the dynamics of dipole-mediated energy transport by interaction-enhanced imaging, Science **342**, 954 (2013).

[17] E. Brion, L. H. Pedersen, and K. Mølmer, Implementing a neutral atom Rydberg gate without populating the Rydberg state, J. Phys. B **40**, S159 (2007).

[18] M. Müller, I. Lesanovsky, H. Weimer, H. P. Büchler, and P. Zoller, Mesoscopic Rydberg Gate Based on Electromagnetically Induced Transparency, Phys. Rev. Lett. **102**, 170502 (2009).

[19] L. Isenhower, E. Urban, X. L. Zhang, A. T. Gill, T. Henage, T. A. Johnson, T. G. Walker, and M. Saffman, Demonstration of a Neutral Atom Controlled-NOT Quantum Gate, Phys. Rev. Lett. **104**, 010503 (2010).

[20] E. Kuznetsova, T. Bragdon, R. Côté, and S. F. Yelin, Cluster-state generation using van der Waals and dipole-dipole interactions in optical lattices, Phys. Rev. A **85**, 012328 (2012).

[21] T. Xia, X. L. Zhang, and M. Saffman, Analysis of a controlled phase gate using circular Rydberg states, Phys. Rev. A **88**, 062337 (2013).

[22] M. M. Müller, M. Murphy, S. Montangero, T. Calarco, P. Grangier, and A. Browaeys, Implementation of an experimentally feasible controlled-phase gate on two blockaded Rydberg atoms, Phys. Rev. A **89**, 032334 (2014).

[23] M. H. Goerz, E. J. Halperin, J. M. Aytac, C. P. Koch, and K. B. Whaley, Robustness of high-fidelity Rydberg gates with single-site addressability, Phys. Rev. A **90**, 032329 (2014).

[24] T. Keating, R. L. Cook, A. M. Hankin, Y.-Y. Jau, G. W. Biedermann, and I. H. Deutsch, Robust quantum logic in neutral atoms via adiabatic Rydberg dressing, Phys. Rev. A **91**, 012337 (2015).

[25] D. D. Bhaktavatsala Rao and K. Mølmer, Robust Rydberg-interaction gates with adiabatic passage, Phys. Rev. A **89**, 030301(R) (2014).

[26] K. M. Maller, M. T. Lichtman, T. Xia, Y. Sun, M. J. Piotrowicz, A. W. Carr, L. Isenhower, and M. Saffman, Rydberg-blockade controlled-NOT gate and entanglement in a two-dimensional array of neutral-atom qubits, Phys. Rev. A **92**, 022336 (2015).

[27] S. Das, A. Grankin, I. Iakoupov, E. Brion, J. Borregaard, R. Boddeda, I. Usmani, A. Ourjoumtsev, P. Grangier, and A. S. Sørensen, Photonic controlled-PHASE gates through Rydberg blockade in optical cavities, Phys. Rev. A **93**, 040303(R) (2016).

[28] E. Brion, A. S. Mouritzen, and K, Mølmer, Conditional dynamics induced by new configurations for Rydberg dipole-dipole interactions, Phys. Rev. A **76**, 022334 (2007).

[29] H. Z. Wu, Z. B. Yang, and S. B. Zheng, Implementation of a multiqubit quantum phase gate in a neutral atomic ensemble via the asymmetric Rydberg blockade, Phys. Rev. A **82**, 034307 (2010).

[30] L. Isenhower, M. Saffman, and K. Mølmer, Multibit C_k NOT quantum gates via Rydberg blockade, Quantum Inf. Process. **10**, 755 (2011).

[31] M. A. Nielsen and I. L. Chuang, *Quantum Computation and Quantum Information* (Cambridge University Press, Cambridge, 2000).

[32] C. Ates, T. Pohl, T. Pattard, and J. M. Rost, Antiblockade in Rydberg Excitation of an Ultracold Lattice Gas, Phys. Rev. Lett. **98**, 023002 (2007).

[33] T. Amthor, C. Giese, C. S. Hofmann, and M. Weidemüller, Evidence of Antiblockade in an Ultracold Rydberg Gas, Phys. Rev. Lett. **104**, 013001 (2010).

[34] T. Pohl and P. R. Berman, Breaking the Dipole Blockade: Nearly Resonant Dipole Interactions in Few-Atom Systems, Phys. Rev. Lett. **102**, 013004 (2009).

[35] J. Qian, Y. Qian, M. Ke, X. L. Feng, C. H. Oh, and Y. Z. Wang, Breakdown of the dipole blockade with a zero-area phase-jump pulse, Phys. Rev. A **80**, 053413 (2009).

[36] Z. C. Zuo and K. Nakagawa, Multiparticle entanglement in a one-dimensional optical lattice using Rydberg-atom interactions, Phys. Rev. A **82**, 062328 (2010).

[37] T. E. Lee, H. Häffner, and M. C. Cross, Collective Quantum Jumps of Rydberg Atoms, Phys. Rev. Lett. **108**, 023602 (2012).

[38] A. W. Carr and M. Saffman, Preparation of Entangled and Antiferromagnetic States by Dissipative Rydberg Pumping, Phys. Rev. Lett. **111**, 033607 (2013).

[39] L. Sárkány, J. Fortágh, and D. Petrosyan, Long-range quantum gate via Rydberg states of atoms in a thermal microwave cavity, Phys. Rev. A **92**, 030303(R) (2015).

[40] S. L. Su, E. J. Liang, S. Zhang, J. J. Wen, L. L. Sun, Z. Jin, and A. D. Zhu, One-step implementation of the Rydberg-Rydberg-interaction gate, Phys. Rev. A **93**, 012306 (2016).

[41] D. F. V. James and J. Jerke, Effective Hamiltonian theory and its applications in quantum information, Can. J. Phys. **85**, 625 (2007).

[42] S. M. Tan, A computational toolbox for quantum and atomic optics, J. Opt. B **1**, 424 (1999).

[43] More precisely, the transition $|r0(r1)\rangle \rightarrow -i|10(11)\rangle$ is achieved. However, the desired transitions can be realized by setting the relative phase between the laser pulse of step 1 and that of step 3 to π. On the other hand, by switching the encoding energy level $|0\rangle \leftrightarrow |1\rangle$ of atom 2, one can also get the desired quantum logic gate without modulating the relative phase.

[44] M. A. Nielsen, A simple formula for the average gate fidelity of a quantum dynamical operation, Phys. Lett. A **303**, 249 (2002).

[45] A. G. White, A. Gilchrist, G. J. Pryde, J. L. O'Brien, M. J. Bremner, and N. K. Langford, Measuring two-qubit gates, J. Opt. Soc. Am. B **24**, 172 (2007).

[46] W. Li, C. Ates, and I. Lesanovsky, Nonadiabatic Motional Effects and Dissipative Blockade for Rydberg Atoms Excited from Optical Lattices or Microtraps, Phys. Rev. Lett. **110**, 213005 (2013).

[47] M. Saffman and T. G. Walker, Analysis of a quantum logic device based on dipole-dipole interactions of optically trapped Rydberg atoms, Phys. Rev. A **72**, 022347 (2005).

[48] M. Cozzini, T. Calarco, A. Recati, and P. Zoller, Fast Rydberg gates without dipole blockade via quantum control, Opt. Commun. **264**, 375 (2006).

[49] W. Li, P. J. Tanner, and T. F. Gallagher, Dipole-Dipole Excitation and Ionization in an Ultracold Gas of Rydberg Atoms, Phys. Rev. Lett. **94**, 173001 (2005).

[50] T. Amthor, M. Reetz-Lamour, S. Westermann, J. Denskat, and M. Weidemüller, Mechanical Effect of Waals Interactions Observed in Real Time in an Ultracold Rydberg Gas, Phys. Rev. Lett. **98**, 023004 (2007).

[51] T. Amthor, M. Reetz-Lamour, C. Giese, and M. Weidemüller, Modeling many-particle mechanical effects of an interacting Rydberg gas, Phys. Rev. A **76**, 054702 (2007).

[52] X. L. Zhang, L. Isenhower, A. T. Gill, T. G. Walker, and M. Saffman, Deterministic entanglement of two neutral atoms via Rydberg blockade, Phys. Rev. A **82**, 030306(R) (2010).

[53] J. H. Yang, X. D. He, R. J. Guo, P. Xu, K. P. Wang, C. Sheng, M. Liu, J. Wang, A. Derevianko, and M. S. Zhan, Coherence Preservation of a Single Neutral Atom Qubit Transferred Between Magic-Intensity Optical Traps, Phys. Rev. Lett. **117**, 123201 (2016).

[54] T. Macrì and T. Pohl, Rydberg dressing of atoms in optical lattices, Phys. Rev. A **89**, 011402(R) (2014).